tron microprobe is convenient because it can be attached to a scanning electron microscope. Its lateral-resolution dimension is much larger than the probe-beam diameter, however, because of beam scattering and spreading beneath the surface. The depth of the analyzed volume is determined by the hundreds-of-nanometer penetration depth of the ~10-keV probe beam. When the film is thinner than this, elements in the substrate will also be seen, while the sensitivity to film elements will be reduced. For accurate quantitative analysis of such films, one needs a calibration sample having the same thickness as well as a similar composition to that of the unknown. On the other hand, **x-ray fluorescence** can be made to analyze only the top 10 nm or so by directing the x-ray probe beam at grazing incidence so that total external reflection occurs. This technique has very high sensitivity exceeded only by mass spectrometry, but it requires a large sample diameter of 10 mm and is not sensitive to elements lighter than S. Moreover, if the surface is not absolutely flat, reflection is not total and the ratio of surface to subsurface sensitivity drops.

10.2.2 Mass spectrometry

Here, vapor is ionized and then separated according to particle mass-to-charge ratio (q/m) using a **quadrupole** electric field or a **magnetic** field. For analysis of sputter-volatilized solids such as thin films, sensitivity is better than 1 ppb (part per billion, or 10^{-9}) for some elements, so it is very good for detecting trace contaminants, although it is less accurate than other techniques having less sensitivity.

In **secondary-ion mass spectrometry** (SIMS), an ion beam sputters away the film, and the small fraction that is sputtered as ions rather than as neutrals is analyzed. This fraction varies by orders of magnitude depending on ion-beam element, sputtered element, and film composition (the matrix effect). Even with calibration samples, it is difficult to obtain accuracy of better than a factor of two, although sensitivity is very high. Depth resolution is the same as in XPS and Auger and for the same reasons. Lateral resolution of 1 μm can be obtained by imaging the pattern of sputtered ions onto a position-sensitive ion detector.

In **glow-discharge mass spectrometry**, a plasma over the sample is used to sputter it (see Sec. 9.3.3). Sensitivity is even higher than in SIMS because of larger sample area and ionization of the vapor in the plasma, but depth resolution is poor.

10.2.3 Rutherford backscattering

Rutherford backscattering spectrometry (RBS) [10] is basically billiard-ball physics and is therefore the most quantitative of the elemental-analysis techniques discussed here. Relative sensitivity from element to element and matrix effects can be calculated accurately from first principles without the use of calibration samples. In RBS, a beam of He^{++} (alpha particles) is directed at the sample at high enough energy (≈2 MeV) so that the particles scatter from the sample's atomic nuclei in binary Coulomb collisions unscreened by the surrounding electron clouds (Rutherford scattering). Screened collisions of ions at lower energy are more complicated and were discussed in Sec. 8.5.2.2. From the energy spectrum of the backscattered particles, elemental concentrations and their depth profiles can be calculated. A target atom scattering the beam withdraws from the He^{++} an amount of energy determined only by the target-atom mass, m_t, and given by Eq. (8.20) corrected for the scattering angle, so that m_t is easily calculated from the kinetic energy remaining in the backscattered beam. Heavy elements withdraw little energy, so they are more difficult to resolve from each other, but the sensitivity for them is much higher because the scattering cross-section increases as atomic number squared.

When the scattering atom is at some depth beneath the surface, additional energy is lost by the ingoing and outgoing beam because of the stopping power of the material for the beam as expressed in Eq. (8.22). Thus, the thicker the film, the broader in energy becomes the backscattered peak from an element that is evenly distributed through it, and variation in peak height with backscattering energy can be used to calculate **depth profile** with a resolution of about 10 nm. Thick films having multiple elements of similar masses will encounter peak-overlap problems, however. Meanwhile, the substrate elements generate a background signal in the energy spectrum which extends all the way from the Eq. (8.20) energy down to zero energy because of the stopping effect. Thus, when a major element in the substrate is heavier than one in the film, the peak from that film element will sit on top of the substrate background, greatly reducing its signal-to-noise ratio. Substrate m_t can be minimized by depositing the film on pyrolytic graphite sheet.

10.2.4 Hydrogen

Hydrogen gives no signal in any of the electron or x-ray spectroscopies, because it has no inner-shell electrons. Also, it is too light to backscatter the beam in RBS. Its bonds do produce absorption peaks in infrared spectroscopy (Sec. 10.1.5), but quantification requires a calibration sample of known H content in the *same bonds* to determine oscillator strength [Eq. (10.3)]. H can be measured by mass spectrometry, but accuracy is poor. The following techniques are useful for quantifying H.

In a modification of RBS sometimes called **forward-recoil scattering**, a 2-MeV He^{++} beam is directed at a grazing angle to the sample surface, so that the H which is scattered forward by the beam has a high probability of escaping from the surface. The sensitivity is about 0.01 at.%.

Hydrogen can be **volatilized** from the sample by sufficient heating. When this is done in a vacuum chamber having a known pumping speed and a calibrated pressure gauge, the amount evolved can be found by integrating Eq. (3.2) over the evolution period. It is important to also monitor the evolution with a mass spectrometer to determine the molecular form of the evolving H and to determine the fraction of the pressure burst that does not contain H. For example, H evolves as H_2 from metals and Si, but as H_2O from silicon dioxide and as H_2 and NH_3 from plasma-deposited silicon nitride. Some of the evolving H may be coming from water desorbed either from the surface or from internal porosity, but this typically evolves at a lower T (<500 K) than the H from within the solid. The sample may have to be heated to as much as 1200 K or so to release all the H from the solid.

Nuclear-reaction analysis can be both sensitive and accurate for H and other light elements (Brundle, 1992), but it requires access to a particle accelerator as well as careful calibration. For example, a beam of the ^{15}N isotope at the specific resonance energy shown here undergoes the reaction

$$H + {}^{15}N(6.385\ MeV) \rightarrow {}^{12}C + {}^{4}He + \gamma(4.43\ MeV) \qquad (10.4)$$

where γ represents gamma rays whose flux can be calibrated for H concentration. This technique has been used to determine H in silicon nitride [11], for example.

10.3 Properties

Film properties refer to the film's interactions with its environment. These interactions determine the film's performance in its application: it is where "the rubber hits the road." Properties are governed by structure and composition, so analysis of all three kinds gives insight into how to modify the deposition process to improve properties. The effects of various deposition parameters on film structure and composition have been a major theme throughout the book.

Film properties were categorized in Table 1.1. In the subsections below, we address optical, electrical, and mechanical properties. **Magnetic properties** are determined by film interaction with a coil such as that in the read/write head of a memory disc. Also, magnetic domains can be mapped with the atomic force microscope by using a magnetic tip to sense magnetic fringe fields. **Chemical properties** mainly involve the film's dissolution rate in various etchants [1].

10.3.1 Optical behavior

A film may reflect, absorb, transmit, or scatter light, and these properties are functions of wavelength. All of the impinging light undergoes one of these four fates. **Reflection and scattering** are measured by the intensity of a light beam returned at the specular angle and at nonspecular angles, respectively. Scattering increases with surface roughness and particulate contamination (Sec. 10.1.2) and, for transparent materials, with bulk inhomogeneity. **Absorption and transmission** from the infrared (IR) to the ultraviolet (UV) regime can be determined by spectroscopy, as discussed for the infrared in Sec. 10.1.5.

The general optical behavior of solids is as follows. Metals reflect and absorb light strongly, because their free electrons prevent electromagnetic-wave propagation. (Compare microwaves in plasmas, Sec. 9.5.1.) The higher the electrical conductivity, the higher is the reflected fraction versus the absorbed fraction because of the shallower "skin depth" [Eq. (9.43)], which is why Ag makes the best mirrors. Nonmetals absorb light strongly by electron/hole-pair generation at photon energies above the band-gap energy or "fundamental absorption edge," which is in the UV for insulators and in the visible or near-IR for semiconductors. Additional absorption occurs at various wavelengths below the band gap due to defects, impurities, and bond resonances.

The amounts of reflection, absorption, and transmission occurring in nonscattering materials are determined uniquely by the fundamental optical constants of Eq. (4.47): the index of refraction, $\tilde{n}$, and the extinction coefficient, κ. A transparent film's $\tilde{n}$ can be measured by interference oscillations if its thickness is known, and its $\tilde{n}$, κ and thickness can all be determined by ellipsometry. These techniques were discussed in Sec. 10.1.1.

10.3.2 Electrical behavior

Here, the analytical techniques and the properties measured differ for metals, semiconductors, and insulators (dielectrics). For metals, the basic electrical property is the **resistivity**, ρ (Ω-cm), of the bulk material, which is defined as the resistance, R (Ω), of a 1-cm cube of material between opposite faces. With thin films, it is more convenient to think in terms of the resistance of a square of film between opposite edges, as shown in Fig. 10.8. This resistance is known as the "sheet resistivity" and is given in ohms per square,

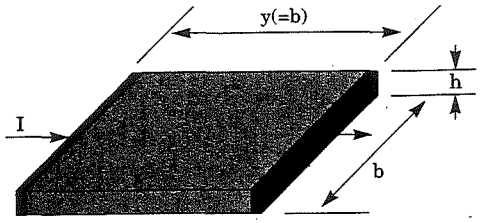

Figure 10.8 Geometry defining the sheet resistivity of a film of thickness h.

$$\rho_s\ (\Omega/\square) = \rho y/A = \rho/h \qquad (10.5)$$

where h is the film thickness and A is the cross-sectional area of the conduction path, bh. Note that ρ_s is independent of the size of the square, so that the R of a conducting thin-film line is just proportional to the number of squares represented by the y/b ratio of the line. The value of ρ_s is conveniently measured with the linear four-point probe shown in Fig. 10.9, provided that the substrate has high enough ρ so that most of the current, I, passes through the film. By measuring the voltage drop, V, with a different pair of probes than the pair used for current flow, the voltage drop associated with current flow through the contacts is removed from the measurement, and only the voltage drop across a distance d of film is measured. The input impedance of the voltmeter must be much higher than the film resistance across the distance d so that it does not provide a shunt path for current flow. The four-point arrangement makes the quality of the probe contacts noncritical, so long as they can pass enough current to generate a measurable V. Thus, they can usually be just point contacts placed under pressure by a spring-loaded probe jig. For equal probe spacing, ρ_s is given simply by [12]

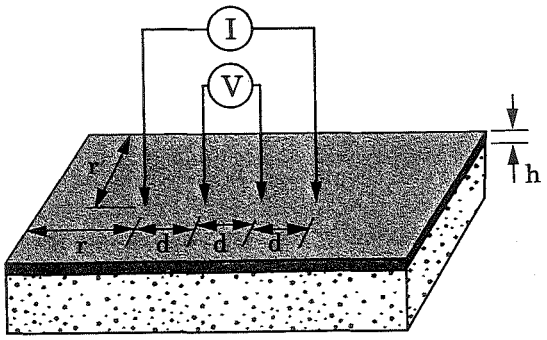

Figure 10.9 Linear four-point probe for sheet-resistivity measurement of a film on an insulating substrate.

$$\rho_s = \frac{\pi}{\ln 2}\frac{V}{I} = 4.53\frac{V}{I} = 4.53\ R \qquad (10.6)$$

For good accuracy, the contact diameter should be much smaller than d, and the distance, r, from the edge of the probe array to the edge of the film should be much larger than d. For example, when r/d = 15, measured ρ_s is 1 percent higher than actual ρ_s, and when r/d = 6, it is 10% higher [12]. When film thickness is also known, ρ can be calculated from ρ_s by Eq. (10.5) and compared with the known ρ of the bulk material as a measure of film quality. However, very thin films of h < 10 nm or so have ρ_s increased by surface and interface scattering of the conducting electrons [2].

The ρ_s of semiconductor films can also be measured with the linear probe array, but it is more common to use the square "van der Pauw" array [13] of Fig. 10.10*a* or *c*. This way, one can separately obtain the **electron mobility and concentration**, μ_e and n_e (or μ_h and n_h for hole conduction), whose product determines the conductivity, s = $1/\rho$ [see Eq. (6.2)]. For ρ_s measurement, the current and voltage contacts are configured in parallel as in Fig. 10.10*a*, so that a resistance $R_{AB,CD} = V_{DC}/I_{AB}$ is obtained. Then, the array is rotated 90° to obtain $R_{BC,AD}$. If pattern asymmetry is small enough that these two R values are within 30 percent of each other, then the average R is related to ρ_s by Eq. (10.6) (to within 1 percent), just as for the linear probe. The contacts need to be at the periphery of the film and much smaller in diameter than the distance between them to avoid measurement errors. The geometry of Fig. 10.10*c* is less susceptible to these errors, but it requires delineation by etching. The film periphery may actually be of any shape that has reasonable four-fold symmetry.

The "Hall mobility," μ_H, is obtained from the same contact array using the perpendicular current and voltage configuration of Fig. 10.10*b*. Upon application of a magnetic field, **B**, perpendicular to the film, charge carriers making up the current I_{AC} are deflected sideways by

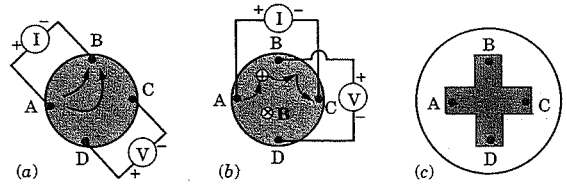

Figure 10.10 Van der Pauw geometries and circuits: (*a*) resistivity configuration, (*b*) mobility configuration with the **B** field pointing into the plane of the figure, and (*c*) patterned film for error reduction.

the Lorentz force, Eq. (8.15), so that they pile up at one or the other voltage contact, depending on the carrier sign, and thus cause a sideways voltage drop V_{BD}. This is the "Hall effect." The deflection in Fig. 10.10*b* is shown for positive charge carriers (holes). Upon reversing **B**, the Hall voltage inverts, and the voltage difference between reversals, ΔV_{BD}, is measured so as to reduce asymmetry errors. To further reduce error, a second measurement is made with the array rotated 90°, so that two "resistances" are obtained, $\Delta R_{AC,BD}$ (= $\Delta V_{BD}/I_{AC}$) and $\Delta R_{BD,CA}$. Their average, ΔR, is related to μ_H by

$$\mu_H\,(\text{cm}^2/\text{V}\cdot\text{s}) = 10^8 \Delta R/2\mathbf{B}\rho_s \qquad (10.7)$$

for **B** in Gauss, where a field of ~2000 Gauss is typically used. Note that the 10^8 would drop out for μ_H and **B** in SI units. The μ_H can be as much as 30 percent larger than the actual carrier mobility—the μ_e or μ_h given by Eq. (6.2)—depending on material and carrier concentration [14]; but to first order, the two μ values can be assumed to be the same if there is only one carrier type. On the other hand, in "compensated" semiconductors, where both electrons and holes are conducting, the Hall voltage will be partly cancelled out, and the calculation of carrier mobility from μ_H becomes more difficult. Finally, at least for uncompensated material, the carrier concentration, n_e or n_h, can be obtained from μ_e or μ_h using Eq. (6.2). Additional information about the material can be obtained by making ρ_s and μ_H measurements at reduced T, as discussed in Sec. 10.1.6.

We now turn to insulating (dielectric) materials. A dielectric film sandwiched between conducting substrate and overlayer materials forms a parallel-plate capacitor, and the application of an electric field across it can produce a wide range of phenomena in the film, including: charge injection from the conducting layers, charge trapping within the dielectric, ion migration, passage of leakage current, ac power dissipation, expansion and contraction of piezoelectric crystalline films such as ZnO, and permanent polarization of ferroelectrics such as $BaTiO_3$. Here, we focus on capacitor behavior and charge motion. If the overlayer material in our sandwich is patterned into a known area and if the dielectric-film thickness is known, the **dielectric constant**, ε, can be found from Eq. (9.29) upon measuring the sandwich capacitance, C, with a capacitance bridge or an "LCR" meter. The latter measures ac impedance and the phase angle between applied voltage and current, and from these it calculates C and R (as well as inductance, L). In an *ideal* capacitor, the phase angle is 90° and there is no power dissipation, but power dissipation can occur in dielectrics due to leakage current and also, at high frequency, due to

a phase-angle shift, δ, resulting from dissipative charge oscillation within the dielectric. The latter is expressed in terms of the dissipation factor or **loss tangent**, tan δ. By the way, when high C is desired in a thin film, there are available some easily deposited materials of very high ε, such as Ta_2O_5 (ε = 22).

Application of fields of more than a few MV/cm across a dielectric film sandwiched between conducting electrode layers causes charge injection (tunneling) through the interfacial potential barrier from the Fermi level, E_f, of the electrode into the conduction band, E_c, of the dielectric, as shown in the energy diagram of Fig. 10.11 (compare Fig. 6.4). This charge consists of electrons from the negative electrode and sometimes also holes from the positive electrode tunneling into the valence band. The charges may either pass through to the other electrode, causing leakage current, or they may become trapped in defect states deep within the band gap of the dielectric. (*Porous* dielectric films may have conductive pathways through their internal surface area at much lower fields.) At still higher fields, the injected electrons gain enough kinetic energy to cause impact ionization of atoms within the dielectric, and this results in an electron avalanche and dielectric breakdown. This is analogous to the breakdown of gas to form a plasma, as discussed after Eq. (8.14). Leakage behavior and the onset of breakdown is conveniently measured by the **ramp I-V characteristic** of the sandwich. The voltage, V, across the electrodes is increased in steps of ~1 V at intervals of ~1 s, and the leakage current, I, is measured at each step once I recovers from the V step. The stepwise V ramp is preferable to a continuous ramp, because it removes from the measurement the capacitive displacement current that accompanies

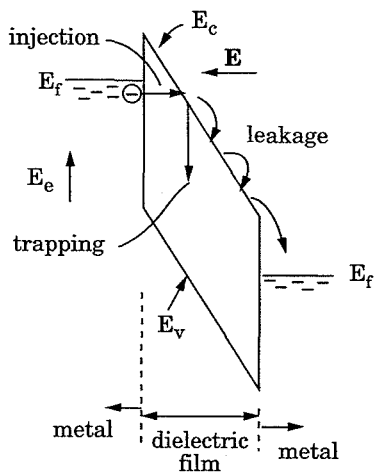

Figure 10.11 Electron potential-energy (E_e) diagram and charge behavior for a dielectric film under high electric field, **E**, between two conductors.

the increasing V [Eq. (9.28)]. In a typical I-V plot, I remains at noise level for awhile and then increases exponentially but smoothly until a sudden large jump in I occurs at a particular V step, which is defined as the breakdown voltage. Good SiO_2 has a breakdown voltage of ≈11 MV/cm, for example. Although the I-V characteristic is a convenient measurement, its shape and the breakdown V can vary with the ramp rate and with the film's electrical-stressing history when charge trapping is occurring, and then it is important to also measure the charge trapping directly.

The amount of charge residing in a dielectric film can be measured if the film is deposited on a lightly n-doped Si wafer and then overcoated with a metal film patterned into mesas to make MIS (metal/insulator/semiconductor) capacitors as shown in Fig. 10.12*a*. When the metal electrode is biased positively with respect to the Si, conduction electrons in the Si accumulate at the dielectric interface so that the capacitance, C, is determined by the dielectric thickness, h. However, under negative bias, electrons are repelled from the interface to a "depletion depth," b, which increases with bias and with decreasing Si doping level. Then, C is determined by the thickness (b + h) and is therefore lower, in accordance with Eq. (9.29). Thus we obtain the characteristic C-V curve shown in Fig. 10.12*b*. [This is the shape when high-frequency modulation of the bias (>10 kHz or so) is used to measure C; at low frequency, C instead rises again under high negative bias in the "inversion" regime where minority-carrier holes are accumulated, because they can respond to slow modulation and thus act as an electrode.] When there is no *net* charge in the dielectric, the transition from electron depletion to accumulation occurs near zero bias. The transition V is known as the "flat-band voltage," because it is where the conduction and valence bands of the Si are bent neither up (depletion) nor down (accumulation) at the interface. When negative charge is trapped in the dielectric, it acts like negative bias on the electrode, causing depletion even with no bias, so that a more positive electrode bias is required to accumulate the Si, and the C-V curve shifts to the right as shown in Fig. 10.12*b*. In quantitative terms, the trapped charge causes an electric-field change across it which is given by Eq. (8.4). Conversely, positive trapped charge causes a C-V shift to the left.

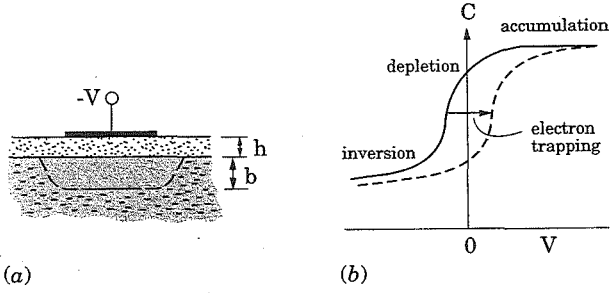

Figure 10.12 MIS-capacitor behavior: (*a*) n-doped semiconductor depletion to depth b under negative metal-electrode bias, and (*b*) high-frequency C-V curve with no charge (solid line) and with negative charge (dashed line) trapped in the dielectric film.

From the amount of the **C-V shift**, one can calculate the concentration of trapped charge as well as its distribution across the dielectric film in the field direction [15]. This technique is very sensitive for measuring the amount of charge trapped. The charge may have been (1) embedded during plasma deposition, (2) diffused in as ionic contaminants during or after deposition, or (3) injected during high-field stressing. Fixed charge in the deposited film (case 1) is revealed by a nonzero flat-band voltage of the initial C-V curve. Ionic contamination (case 2) is often due to Na^+. The presence of minute quantities of this ubiquitous ion in the gate oxide of field-effect transistors frustrated the development of these key devices and thus delayed the establishment of the integrated-circuit industry for many years. Mobile-ion contamination can be distinguished from fixed charge in the dielectric by **"bias-temperature" stressing**, whereby the ions are made to drift at elevated T in a moderate electric field, causing a C-V shift. The tendency of the film to trap electrons injected into it (case 3) is determined by **avalanche injection** of a metered pulse of charge, followed by measurement of the resulting C-V shift [15]. The result can be characterized in terms of the product of the concentration of traps per cm^3 times their cross section in cm^2, $n_t\sigma_t = \alpha_e$ (cm^{-1}), where α_e is essentially an electron absorption coefficient analogous to the one for light defined by Eq. (4.49). When the film is thinner than $1/\alpha_e$, part of the injected charge passes through to the opposite electrode, whereas when it is thicker, all of the charge becomes trapped.

10.3.3 Mechanical behavior

Here, we address four properties: stress, adhesion, hardness, and stiffness.

The level of a film's tensile or compressive **stress** can be determined by the resulting concave or convex curvature in the substrate as given by Eq. (5.57) and discussed in detail there.

Adhesion of a film to its substrate is the most difficult of the four to measure. Simple qualitative tests include determining whether or not the film peels off along with a strip of sticky tape pressed onto it and then pulled off, or whether it chips off upon being scratched with a sty-

lus. A more quantitative test is illustrated in Fig. 10.13. A metal stud of known cross-section, A, is glued to the film, and then a force ramp (F) is applied until something breaks—either the substrate or the glue or the film/substrate interface. Thin substrates can be supported by gluing on a backing plate as shown. A strong glue such as epoxy should be used, since its strength sets the upper limit of measurable adherence strength. Soldering or brazing provides a stronger bond, but the heating may cause interdiffusion or structural change at the interface to be tested. When the film/substrate interface breaks first, the interfacial tensile strength is given directly by F/A. The tensile strength of well cured epoxy is about 80 MPa or 12 kpsi. With multilayer films, the weakest interface will be the one that breaks, of course, and which interface broke can be identified by compositional analysis or sometimes by microscopic inspection. The pull force must be exactly perpendicular to the film surface so as to distribute the tension evenly over A and thereby maximize the breaking force.

Hardness of thin films can be determined by "nanoindentation" [16], a miniaturized version of the Vickers hardness test for bulk materials, in which the point of a pyramidal diamond stylus is pressed into the surface with a specified force. The size of the resulting dimple is inversely related to hardness. The film should be thicker than about 10 times the depth of the dimple so as to avoid substrate influence.

The stiffness of a material is characterized by its **elastic modulus**, Y (Pa), as defined in Eq. (5.50). Y varies with microstructure, so its value in a thin film is not necessarily the same as in the bulk material. The Y of a thin-film material can be found from the resonant frequency of a suspended section of film. The cantilever structure of Fig. 10.14 can be fabricated using microlithography, first to pattern the film into a finger shape and then to undercut-etch a well in the substrate using a second photomask, so as to leave the end of the finger freely suspended. The fundamental resonant frequency of this rectangular cantilever beam of cross section A = bh and uniform mass density ρ_m is related to Y and geometry by the following equation [17]:

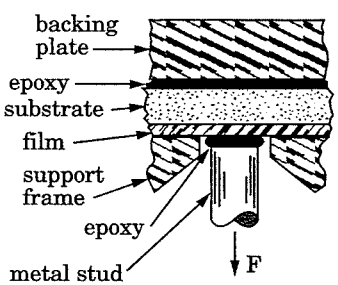

Figure 10.13 Epoxied-stud pull test for film adherence.

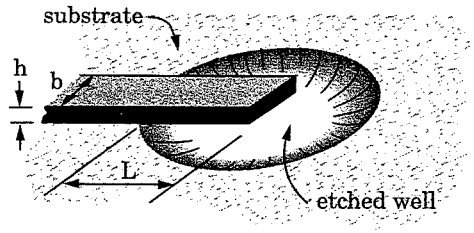

Figure 10.14 Etched-cantilever structure for determining film stiffness.

$$\nu_o = \frac{1.875^2}{2\pi L^2}\sqrt{\frac{YI_z}{\rho_m A}} = 0.162\frac{h}{L^2}\sqrt{\frac{Y}{\rho_m}} \qquad (10.8)$$

in SI units (Pa, kg, m, Hz), where $I_z = bh^3/12$ is the moment of inertia of the beam [compare Eq. (5.56)]. Note that this is a $\sqrt{k/m}$ expression characteristic of mass-spring resonance [Eq. (4.36)]; here, the spring constant $k \propto YI_z/L^3$, and the mass $m \propto \rho_m AL$. The value of ν_o can be found by mounting the Fig. 10.13 structure on a piezoelectric transducer driven by a variable-frequency voltage and watching under a microscope for a blurring of the cantilever upon reaching resonance. The lowest of the various frequencies at which blurring will be seen is the fundamental resonance.

10.4 Conclusion

We have now completed the film-deposition process sequence outlined in Fig. 1.1: source-material supply, transport to the substrate, deposition reactions, and film analysis. The results of analysis contain clues as to how to modify the operation of the first three steps to improve film properties for the desired application. These clues will be more apparent and more numerous if structural and compositional analyses are carried out along with property analysis. Many of the linkages between deposition-process parameters and the nature of the resulting film have been discussed in Chaps. 4 through 9. Still, there are many more linkages to be discovered and new processes to be invented. Hopefully, the information and principles presented in this book will prove to be a useful platform and guide for this endeavor.

10.5 References

1. Walker, P., and W.H. Tarn (eds.). 1991. *CRC Handbook of Metal Etchants*. Boca Raton, Fla.: CRC Press. (Also covers nonmetals.)
2. Berry, R.W., P.M. Hall, and M.T. Harris. 1979. *Thin Film Technology*, Chap. 6, "Electrical Conduction in Metals." Huntington, N.Y.: Krieger Publishing.

3. Sarid, D., and V. Elings. 1991. "Review of Scanning Force Microscopy." *J. Vac. Sci. Technol.* B9:431.
4. Gibson, J.M. 1991. "High Resolution Transmission Electron Microscopy." *MRS Bull.* (March):27.
5. Segmüller, A. 1991. "Characterization of Epitaxial Thin Films by X-ray Diffraction." *J. Vac. Sci. Technol.* A9:2477.
6. Clemens, B.M., and J.A. Bain. 1992. "Stress Determination in Textured Thin Films using X-ray Diffraction." *MRS Bull.* (July):46.
7. Back, D.M. 1991. "Fourier Transform Infrared Analysis of Thin Films." In *Physics of Thin Films* 15, "Thin Films for Advanced Electronic Devices," ed. M.H. Francombe and J.L. Vossen. Orlando, Fla.: Academic Press.
8. Herman, M.A., and H. Sitter. 1989. *Molecular Beam Epitaxy: Fundamentals and Current Status*, Chap. 5. Berlin: Springer-Verlag.
9. Olmstead, M.A., and N.M. Amer. 1983. "A New Probe of the Optical Properties of Surfaces." *J. Vac. Sci. Technol.* B1:751.
10. Chu, W.K., and G. Langouche. 1993. "Quantitative Rutherford Backscattering from Thin Films." *MRS Bull.*, (January):32.
11. Lanford, W.A., and M.J. Rand. 1978. "The Hydrogen Content of Plasma-Deposited Silicon Nitride." *J. Appl. Phys.* 49:2473.
12. Smits, F.M. 1958. "Measurement of Sheet Resistivities with the Four-Point Probe." *Bell System Tech. J.* (May):711.
13. van der Pauw, L.J. 1958. "A Method of Measuring Specific Resistivity and Hall Effect of Discs of Arbitrary Shape." *Philips Res. Rep.* 13:1.
14. Look, D.C. 1990. "Review of Hall Effect and Magnetoresistance Measurements in GaAs Materials and Devices." *J. Electrochem. Soc.* 137:260.
15. Nicollian, E.H., and J.R. Brews. 1982. *MOS (Metal-Oxide-Semiconductor) Physics and Technology*, Chap. 11. New York: Wiley-Interscience.
16. Pharr, G.M., and W.C. Oliver. 1992. "Measurement of Thin Film Mechanical Properties Using Nanoindentation." *MRS Bull.* (July):28.
17. Rothbart, H.A. (ed.) 1964. *Mechanical Design and Systems Handbook*, Table 6.6*b*. New York: McGraw-Hill.

10.6 Recommended Reading

Brundle, C.R., C.A. Evans, Jr., and S. Wilson (eds.) 1992. *Encyclopedia of Materials Characterization: Surfaces, Interfaces, Thin Films*. Boston: Butterworth-Heinemann.

Appendix A
Units

A.1 SI (Système International) Units

These units are self-consistent; that is, all conversion factors are unity. They should be used whenever possible to avoid errors in calculation and to facilitate comparison with other peoples' results. The SI units used in this book include the following:

Quantity	Units	Symbol
Capacitance	farads	F
Charge	coulombs	C
Conductance	siemens	S
Current	amperes	A
Distance	meters	m
Electrical potential	volts	V
Energy	joules	J
Force	newtons	N
Frequency	hertz	Hz
Inductance	henrys	H
Magnetic flux density	tesla	T
Mass	kilograms	kg
Power	watts	W
Pressure	pascals	Pa
Resistance	ohms	W
Temperature	kelvin	K
Time	seconds	s

A.2 Conversion Factors

To convert: From To	To From	Multiply by Divide by
Å	nm	0.1
atm	Pa	1.01×10^{5}
bar	Pa	10^{5}
dynes/cm	N/m (J/m^2)	10^{-3}
dynes/cm^2	Pa	0.1
eV	J	1.60×10^{-19}
eV/mc	kJ/mol	96.3
gauss	tesla (webers/m^2)	10^{-4}
g-cal	J	4.186
psi	Pa	6895
sccm	mc/s	4.48×10^{17}
sccm	Pa·*l*/s	1.84
stones/acre	Pa	0.0154
torr	Pa	133 (=400/3)
u	kg	1.66×10^{-27}

A.3 Equivalent Units

Charge	C = A·s
Energy	J = kg·m^2/s^2 = N · m = W·s = V·A·s = C·V
Force	N = kg·m/s^2
Molecular dose	1 L (langmuir) = 10^{-6} torr·s
Pressure	Pa = N/m^2; μm (microns of Hg) = millitorr; mm Hg = torr

Appendix

B

Vapor Pressures of the Elements

The following figures have been reproduced by permission of the present copyright owner, General Electric Corp., from R. E. Honig and D. A. Kramer (1969), "Vapor Pressure Data for the Solid and Liquid Elements," *RCA Review* 30:285. To cover a wide range of T, log p_V has been plotted versus log T rather than versus 1/T, even though the latter would be more linear in accordance with Eq. (4.13). For each element, available data considered reliable have been fitted to a formula consisting of Eq. (4.13) plus some corrective terms. The authors estimated the reliability of the raw data to be ±20 percent, but it always covered a range narrower than that of the figures (and given in the above reference), so reliability may be less in the extrapolated regions, particularly at very low pressure. If accuracy is critical, more recent literature should be compared.

The first two figures include the more common elements, while the third includes element numbers 21 (Sc), 43 (Tc), 56–72, and >84. Elements X having more than one significant vapor species are labeled "ΣX." Note that the red and white solid phases of P have different p_V values. For the p_V values of alloys and compounds, see the discussion of Ch. 4.

These figures are available as larger wall charts from the American Vacuum Society, New York City.